Development, Control and Recovery of Leading- and Trailing-Edge Vortices in Tandem-Airfoil Configurations

Vom Fachbereich Maschinenbau
an der Technischen Universität Darmstadt
zur
Erlangung des Grades eines Doktor-Ingenieurs (Dr.-Ing.)
genehmigte

D i s s e r t a t i o n

vorgelegt von

David E. Rival, M.Sc.

geb. in Atlanta, USA

Berichterstatter:	Prof. Dr.-Ing. C. Tropea
Mitberichterstatter:	Prof. Dr.-Ing. R. Radespiel
Tag der Einreichung:	10.8.2009
Tag der mündlichen Prüfung:	14.10.2009

Darmstadt 2009
D17

Hiermit versichere ich, die vorliegende Doktorarbeit unter der Betreuung von Prof. Dr.-Ing. C. Tropea nur mit den angegebenen Hilfsmitteln selbständig angefertigt zu haben.

Darmstadt, den 10.8.2009

Abstract

Particle Image Velocimetry (PIV) has been used to uncover the two distinct aerodynamic mechanisms associated with cruise and hover conditions in tandem-airfoil configurations, i.e. dragonfly flight. The studies performed here have been carried out at transitional Reynolds numbers and reduced frequencies corresponding to dragonfly flight, which in turn are relevant to the development of Micro Air Vehicles (MAVs). The associated vortex dynamics of these strongly separated flows have been examined using vortex-tracking, pressure-integration and control-volume methods. To a lesser extent, direct force measurements and URANS-based numerical simulations have been used to support the findings. At first the formation and manipulation of leading-edge vortices (LEVs) and trailing-edge vortices (TEVs) for a single airfoil have been examined using non-sinusoidal kinematics and the theory of optimal vortex formation. Results show that the development of the LEV can be modified without the need for a span-wise flow, contrary to popular belief. In a similar fashion, the TEV can be reduced or even completely mitigated through the superposition of a quick-pitch motion near the bottom of the stroke. Subsequently, the studies of tandem configurations in cruise conditions revealed that the vortex-formation process for the forefoil is strongly influenced by the placement of a hindfoil in its wake, be it static or moving. In strong agreement with observations made on live dragonflies, airfoil configurations with specific out-of-phase kinematics of approximately $\psi = 60^\circ$ were found to generate net thrust. The mechanism for this thrust production was identified as the formation of a leading-edge suction bubble on the hindfoil induced by the passing of the forefoil LEV. Similarly, the passing forefoil TEV was found to induce a vortex on the hindfoil, which in turn helped reduce power consumption on the upstroke. Finally, time-resolved PIV investigations into tandem hovering identified a beneficial interaction at $\psi = 90^\circ$ in which the forefoil TEV interacted with the development of the hindfoil LEV. This aerodynamic mechanism in turn adjusted the strength and positioning of the hindfoil TEV, thus affecting thrust and power consumption. This result agrees with observations in nature and analogous force measurements for three-dimensional flapping wings, suggesting again that a span-wise flow is not necessarily required for efficient vortex control but rather a result of the evolutionary restrictions in nature towards root-flapping flight.

Kurzfassung

Die aerodynamischen Vorgänge, wie sie beim Reise- und Schwebeflug von Libellen vorkommen, wurden mit zwei Profilen in einer Tandemanordnung erzeugt und mit Hilfe von Particle Image Velocimety (PIV) erfasst. Hierbei wurden Reynolds Zahlen im Transitionsbereich und reduzierte Frequenzen untersucht, die den Flügelschlag von Libellen abbilden und somit für die Entwicklung von Micro Air Vehicles (MAVs) relevant sind. Die Dynamik der Wirbelstrukturen, die sich in den stark abgelösten Strömungen über den Profilen bilden, wurde durch die Berechnung der Trajektorien der Wirbelzentren, der Druckintegrale und der Kontrollvolumenmethode analysiert. Weiterhin wurden Kraftmessungen und numerische Simulationen (URANS) durchgeführt, um die Ergebnisse abzusichern. Als erstes wurden Entstehung und Beeinflussung der Vorderkanten- und Hinterkantenwirbel an einem einzelnen Profil untersucht, indem eine nicht-sinusförmige Kinematik und das Konzept der optimalen Wirbelbildung angewendet wurden. Entgegen der gängigen Meinung, zeigen die Ergebnisse, dass der Vorderkantenwirbel ohne das Vorhandensein einer Strömungskomponente in Querrichtung beeinflusst werden kann. Ebenso kann der Hinterkantenwirbel durch die Überlagerung einer schnellen Nickbewegung im Tiefpunkt der Hubbewegung reduziert oder sogar komplett getilgt werden. Die darauf aufbauende Analyse der Strömung, die sich in der Tandemanordnung ergibt, zeigt für den Reiseflug, dass die Wirbelbildung am vordern Profil stark durch die Position des hinteren Profils beeinflusst wird. Dies gilt sowohl für den Fall, in dem das hintere Profil statisch ist, als auch, wenn es ebenfalls bewegt wird. Messungen bei verschiedenen Phasenwinkeln zwischen den Profilen haben gezeigt, dass bei einem Phasenwinkel von $\psi = 60°$ in der Summe ein Schub entsteht, was in Übereinstimmung mit Beobachtungen aus dem Libellenflug ist. Der für den Schub verantwortliche Mechanismus, konnte als eine Tiefdruck-Blase am hinteren Profil, die durch den vorüberziehenden Vorderkantenwirbel des vorderen Profils verursacht wird, identifiziert werden. In gleicher Weise entsteht durch das Vorüberziehen des Hinterkantenwirbels des vorderen Profils ein induzierter Wirbel am hinteren Profil, der den Energieverbrauch innerhalb der Aufwärtsbewegung verringert. Abschlieend wurde die Strömung, die sich für die Tandemanordnung im Schwebeflug ergibt, mit Hilfe von zeitaufgelösten PIV-Messungen erfasst. Hierbei ergab sich, in Übereinstimmung mit den Erkenntnissen von Libellen, ein Phasenwinkel von $\psi = 90°$, bei dem der Hinterkantenwirbel des vorderen Profils eine positive Wirkung auf die Entstehung des Vorderkantenwirbels des hinteren Profils hat. Dieser Mechanismus bestimmt die Stärke und Position des Hinterkantenwirbels am hinteren Profil und beeinflusst dadurch die Schuberzeugung und den Energieverbrauch. Diese Ergebnisse stimmen sowohl mit den Beobachtungen in der Natur, als auch mit Kraftmessungen an dreidimensionalen Schlagflügelmodellen überein. Dies legt die Vermutung nahe, dass die Strömungskomponente in der Querrichtung des Flügels nicht für eine effektive Kontrolle der Wirbelstrukturen notwendig ist, sondern aus den Einschränkungen bei der evolutionären Entwicklung von Schlagflügel herrührt.

Acknowledgements

This research was supported by the Deutsche Forschungsgemeinschaft (German Research Foundation) within the national priority program entitled *Nature-Inspired Fluid Mechanics* (SPP1207, Tr 194/40).

First and foremost I would like to acknowledge the support and guidance of my advisor Prof. Dr.-Ing. Cam Tropea. Even before arriving in Germany in January 2006 he had already begun inspiring me through our regular correspondence. Over the years, Professor Tropea entrusted me with a great deal of responsibility, which in turn helped develop my confidence and hone my research skills. I have grown quite a bit under his guidance over the last four years.

I would also like to thank Prof. Dr.-Ing. Rolf Radespiel from the Technische Universität Braunschweig for refereeing this thesis and for his constructive input over the course of the NATO Research and Technology Organization program entitled: *AVT-149 Task Group on Unsteady Low Reynolds Number Aerodynamics for Micro Air Vehicles*. I am also indebted to the chair of this task group, Dr. Michael Ol from the Air Force Research Laboratories at Wright-Patterson AFB, for his feedback over the course of this project.

I am very thankful for having had the opportunity to work with a group of talented students during the course of my stay at the institute. The following students contributed greatly to the research program: Julien Dumond (École Centrale de Lyon), Kai Aschmoneit, Martin Sharman (U. of Glasgow), Tim Prangemeier, Roland Manejev, Dirk Schönweitz and Guillermo Hass (in conjunction with the U. of Toronto). Without their hard work and creativity, many of the results in this thesis would not have materialized. I would also like to extend my thanks to Marc Wolf and Jake (a.k.a. Riley) Monsour for their help with the experiments.

The success of the numerous experimental campaigns in the wind tunnel was in large part due to support from Ilona Kaufhold and her team of machinists who were always prepared to help out in some form or another. From the IT side, Dipl.-Ing. Matthias Quade always showed enormous patience with me, irrespective of the problem or its source. From an administrative standpoint, Silke Wallner and Stephanie Lath at the Lichtwiese provided a great deal of support throughout the course of my stay here in Germany.

The list of colleagues who provided advice over the years is a long one and includes: Dr. Tatjana Hubel, Dr.-Ing. Sven Grundmann, Dr.-Ing. Markus Gnirss, Dr.-Ing. Feras Batarseh, Dipl.-Ing. Jochen Kriegseis and Dipl.-Ing. Benjamin Lambie. A particular thanks goes out to Dipl.-Ing. Matthias Kinzel for his support and friendship. Be it a discussion on Particle Image Velocimetry or a spot at the gym, he was always there to lend a helping hand.

Finally, I would like to acknowledge the encouragement I have received over the years from all my friends and family (wherever they might be hiding), especially from my mom, Rob, Katia, Claudia and Johnny.

Contents

List of Figures

List of Tables

Symbol	Unit	Description
A	m^2	vortex integration window
c	m	chord length
C_d	-	sectional drag coefficient, $2d/\rho U_\infty^2 c$
C_l	-	sectional lift coefficient, $2l/\rho U_\infty^2 c$
C_m	-	sectional moment coefficient, $2m/\rho U_\infty^2 c^2$
C_n	-	sectional normal coefficient, $2n/\rho \dot{h}_{max}^2 c$
C_p	-	pressure coefficient, $2(p-p_\infty)/\rho U_\infty^2 c$
C_P	-	sectional power coefficient, $2P/\rho U_\infty^3 c$
C_t	-	sectional thrust coefficient, $2t/\rho \dot{h}_{max}^2 c$
d	N	sectional drag force
f	Hz	motion frequency
f_{pro}	Hz	quick-pitch pronation frequency
f_{sup}	Hz	quick-pitch supination frequency
h_0	m	plunge amplitude
$h(t)$	m	plunge position
$\dot{h}$	m/s	plunge velocity
$\dot{h}_{max}$	m/s	maximum plunge velocity
k	-	reduced frequency, $\pi f c/U_\infty$
k	m^2/s^2	turbulent kinetic energy
l	N	sectional lift force
m	Nm	sectional aerodynamic moment
p	N/m^2	pressure
p_∞	N/m^2	free-stream pressure
P	Nm/s	power
Re	-	Reynolds number, $U_\infty c/\nu$
Re_t	-	turbulent Reynolds number, $k/\nu\omega$
s	m	airfoil span
S	m	airfoil spacing
t	s	time
t_{pause}	s	duration of pause
t_{pro}	s	beginning of pronation
$t_{<stall}$	s	crossing of static-stall angle
t_{sup}	s	end of supination
t	N	sectional thrust force
T	s	period
Tu	-	turbulence intensity
U_∞	m/s	free-stream velocity
u	m/s	stream-wise velocity
v	m/s	normal velocity
w	m/s	span-wise velocity
x	m	stream-wise direction
y	m	normal direction
z	m	span-wise direction

Greek Letters

Symbol	Unit	Description
α	$^\circ$	angle of attack
α_o	$^\circ$	mean angle of attack
α_1	$^\circ$	pitch amplitude
$\alpha_{eff}(t)$	$^\circ$	effective angle of attack
$\alpha_{geo}(t)$	$^\circ$	geometric angle of attack
$\alpha_{plunge}(t)$	$^\circ$	effective angle of attack for pure plunge
δ_{ij}	-	Kronecker delta
η_P	-	thrust efficiency
Γ	m^2/s	circulation
Γ_{TEV}	m^2/s	TEV circulation
ρ	kg/m^3	density
ν	m^2/s	kinematic viscosity
ν_t	m^2/s	eddy viscosity
ϕ	$^\circ$	phase between pitch and plunge
ψ	$^\circ$	airfoil phasing
ω	$1/s$	specific dissipation rate
ω_z	$1/s$	spanwise vorticity component

Subscripts

Symbol	Description
i, j	indices
F	forefoil
H	hindfoil

Abbreviations

Symbol	Description
CFD	computational fluid dynamics
DES	detached eddy simulations
LCTM	local correlation-based transition model
LES	large eddy simulations
LEV	leading-edge vortex
PIV	particle image velocimetry
RANS	Reynolds averaged Navier-Stokes
SST	shear stress transport
TEV	trailing-edge vortex

1 Introduction

1.1 Overview

As the title suggests, this thesis concerns itself with the behavior of leading-edge vortices (LEVs) and trailing-edge vortices (TEVs) in the context of tandem-airfoil configurations, i.e. dragonfly flight. A particular focus has been placed on the vortex dynamics, including the concepts of optimal vortex formation and blade-vortex interaction with the goal to better understand the thrust production and power reduction. In the first few chapters an overview of the state-of-the-art as well as descriptions of the experimental and numerical methods are provided. Thereafter in chapters 5, 6 and 7, studies focused on single-airfoil kinematics are performed. In chapters 8 and 9, blade-vortex interaction for a static and moving hindfoil is investigated, respectively. In chapter 10, vortex interaction for a hovering configuration is studied. Finally, in chapter 11, the results from the various studies are compiled together to allow for general conclusions to be made regarding the vortical interactions associated with tandem configurations.

1.2 Inspiration from Nature

Biologists over several decades have examined the specific wing kinematics of dragonflies and have uncovered distinct patterns associated with various flight maneuvers. These studies include those by: Norberg (1975); Alexander (1984); Azuma et al (1985); Azuma and Watanabe (1988); Rueppell (1989); Thomas et al (2004); Wang and Russell (2007). Very little regarding the aerodynamic mechanisms themselves could, however, be extracted from these above-mentioned studies. Although present-day dragonflies fly with Reynolds numbers on the order of $Re = \mathcal{O}(10^3)$, dragonflies from the Carboniferous and Permian periods, such as *Meganeuropsis permiana* with its giant wingspan up to 75cm, flew well into the (laminar-to-turbulent) transitional Reynolds-number regime, as reported on in Beckemeyer (2006). Thus dragonfly scaling and their overall efficient and highly-maneuverable flight provide a source of great inspiration to aerodynamicists struggling to uncover the nuances of biological flight.

1.3 Motivation from Engineering

Accompanied with an ever-growing interest in Micro Air Vehicle (MAV) development based on bio-inspired flight, i.e. combined lift and propulsion from flapping wings, lies the challenging goal to scale down such vehicles to lower Reynolds numbers ($Re < 50000$), as reported on by Pines and Bohorquez (2006). In such low Reynolds-number regimes, one of the major limitations is the separation-prone nature of the laminar boundary layer when faced with an adverse pressure gradient. Such a fundamental limitation on an airfoil's performance at these Reynolds numbers was investigated on a laminar profile using force measurements and smoke visualization by Mueller and Batill (1982). More recently Ol et al (2005) examined the transition to turbulence and the position of a laminar separation bubble for low angles of incidence and at $Re = 60000$. Performance

has been found to drop quite dramatically at these Reynolds numbers, where the laminar-to-turbulent transition and therefore reattachment occur very late, if at all.

At these transitional Reynolds numbers relatively little work has been performed to-date to understand the performance of the flapping tandem arrangement inspired by dragonfly flight. Most notable are the studies by Jones and Platzer (1999) and Warkentin and DeLaurier (2007) in which various arrangements including a plunging/flapping forewing and stationary hindwing were investigated. Such an arrangement is based on the development of Schmidt (1965) in which the oscillatory wake of the forewing would allow for thrust generation on the hindwing. One immediate benefit of such a tandem arrangement for MAVs is the potential improvement in flight stability where out-of-phase flapping could significantly dampen cyclic lift production as well as inertial fluctuations of individual wings.

Coincidentally, such aerodynamic interactions are today receiving much attention in the context of energy harvesting. Examples of such devices are so-called *wingmills*, as described in McKinney and DeLaurier (1981), Kinsey and Dumas (2006) and Platzer et al (2009). Other applications include small-scale wind energy production using vertical-axis wind turbines (VAWTs), which can benefit from these vortical interaction effects, as described in Bertenyi et al (2007). The issue of gust response on larger horizontal-axis wind turbines is also of relevance here, see Barlas and van Kuik (2007).

1.4 Objectives

At the onset of this research project, a number of outstanding questions pertaining to vortex development and vortex interactions in tandem configurations were identified. Naturally the objective was to answer as many of these questions as possible, as well as to tie in the results into some general conclusions relating to dragonfly flight. Some of the most pertinent questions addressed in this thesis include:

- How does the vortical wake behind a pure-plunging or pure-pitching airfoil vary with increasing reduced frequency?
- To what extent can dynamic stall increase the loading on a moving airfoil?
- Is a span-wise flow an absolute requirement to stabilize the LEV or can specific two-dimensional kinematics be used to control the formation process?
- Can the strength of the TEV be reduced without influencing the size and strength of the LEV?
- What is the influence of a static or moving hindfoil on the vortex formation process over the forefoil?
- How does the vortical wake of the forefoil influence the flow field and loading on the hindfoil?
- Does the mechanism of vortex interaction vary between cruise and hover conditions?
- Which airfoil phasings are beneficial for cruise and hover conditions and what are the aerodynamic mechanisms responsible for these interactions?

2 Background

2.1 Characterization of Dragonfly Flight

Over the past decades a great deal of analytical, numerical and experimental investigations into tandem-wing aerodynamics, almost exclusively for hover conditions, have been performed with the hope of better understanding the complex aerodynamic interaction associated with dragonfly flight. Among these investigations, Bosch (1978); Lan and Sun (2001); Sun and Lan (2004); Wang and Sun (2005) considered the problem from a two-dimensional standpoint with either the assumption of inviscid or laminar flow. Isogai et al (2004); Maybury and Lehmann (2004); Yamamoto and Isogai (2005); Usherwood and Lehmann (2008); Lehmann (2008, 2009) all investigated the interaction in three dimensions, primarily using force measurements and to a lesser extent particle image velocimetry (PIV). Certain researchers have shown that through wake capture, large increases in performance are attainable for single wings flapping independently, suggesting that the tandem interaction is only secondary in importance. These studies include: Savage et al (1979); Gustafson and Leben (1991); Anderson et al (1998); Birch and Dickinson (2003), in which some go as far as arguing that dragonfly flight is a function of single-wing wake capture and not of vortex interaction between two staggered wings. On the other hand, Scharpf and Mueller (1992) showed that even for static tandem configurations at low Reynolds numbers, drag reduction and lift augmentation existed for several stagger and gap configurations.

Thus a very broad range of explanations for the unsteady aerodynamic mechanisms in dragonfly flight exist, where some claim that the performance is linked to the stabilization of the span-wise (three-dimensional) flow in the leading-edge vortex (LEV), see Ellington (2006); Lehmann (2009). In contrast Thomas et al (2004) have argued that dragonflies use a quasi two-dimensional dynamic stall mechanism during both cruising and accelerating flight, with a LEV over the airfoil on the downstroke and attached flow on the upstroke, as shown by the topology in Fig. 2.1. Thus by no means does a universal explanation for the unsteady aerodynamic mechanisms associated with dragonfly flight exist at the present time.

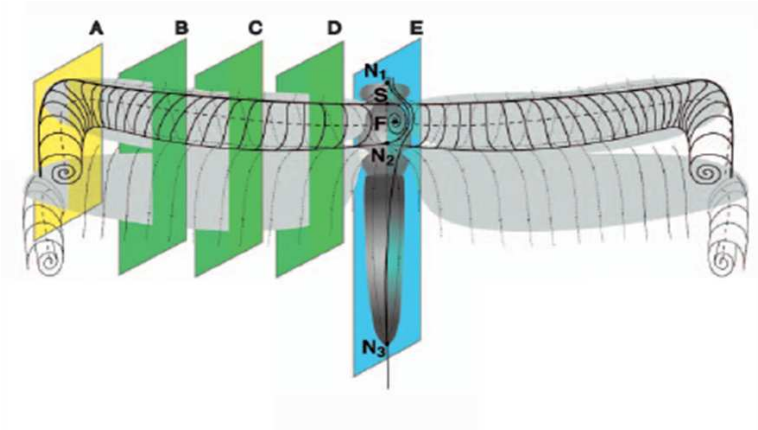

Figure 2.1: Topology of LEV on dragonfly forewings, from Thomas et al (2004).

2.1.1 Cruise versus Hover

By studying the kinematics of live dragonflies, Alexander (1984) observed that in-phase flapping was used for high-lift maneuvers such as take-off, whereas out-of-phase flapping was common for steady-state flight conditions where energetics were a consideration. In fact Azuma and Watanabe (1988), among others, recognized that dragonflies modulated not their flapping frequency but their forewing/hindwing phasing (ψ) depending on their flight speed, i.e. transition from hover to cruise conditions. This phasing was found to vary from $60° \leq \psi \leq 90°$, with lower frequencies observed in hover and higher frequencies found for cruise flight.

In Fig. 2.2 another defining character of dragonfly flight is demonstrated by the tilting of the body axis to the horizontal (body attitude) such that the fore- and hindwing stroke planes approach vertical and horizontal configurations in cruise and hover conditions, respectively. These two extreme flight conditions have been investigated in chapters 9 and 10, which can be considered the bounding limits to the dragonfly's flight envelope.

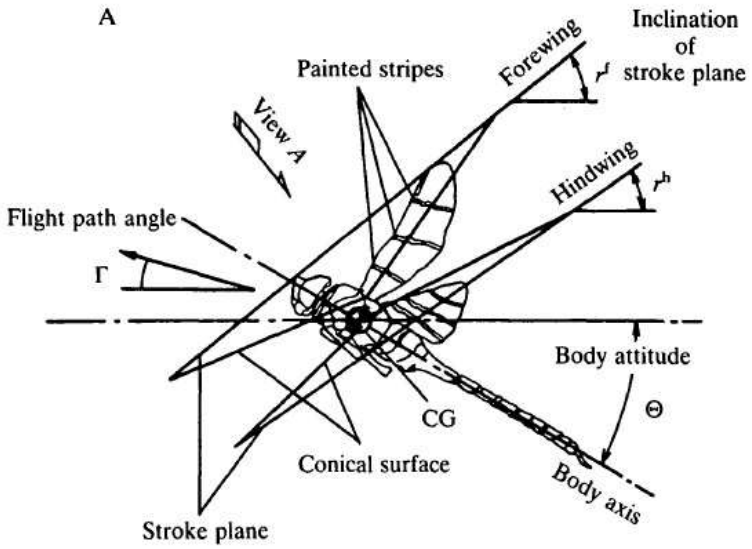

Figure 2.2: Kinematics of dragonfly flight demonstrating the tilting of the body axis (body attitude) to the horizontal, from Azuma and Watanabe (1988).

Thus these two bounding flight conditions, cruise and hover, define also the character of the dragonfly's flow field. In cruise conditions the dragonfly has been observed to combine out-of-phase flapping with intermittent gliding, as reported by Rueppell (1989), where intermittent separation due to dynamic stall on the wings' suction sides is expected. Here maximum thrust generation approaches the total drag, i.e. maximum forward speed is achieved. In contrast, hover flight is characterized by the continuous development of leading- and trailing-edge vortices in both stroke directions, amounting to permanently-stalled flow conditions, as reported on by Wang and Sun (2005).

2.2 Separated Flow

Both natural and biomimetic flight occur predominantly at low Reynolds numbers ($Re < 50000$). Mueller and Batill (1982) have shown that at these scales performance is strongly hampered by the separation-prone nature of the laminar boundary layer. Contrary to classical aerodynamics, separation becomes the norm, not the exception. Such a fundamental limitation to the aerodynamics suggests that lift must be generated through un-

steady aerodynamic mechanisms such as dynamic stall, as outlined by Ellington (2006). Dynamic stall, as reported on by McCroskey (1982), consists of the formation and delayed convection of a leading-edge vortex (LEV) over the downstroke, which in turn can be very advantageous to lift production as well as maneuvering. For cruise conditions, as studied in chapters 5 through 9, dynamic stall has been investigated in great detail, first for a single airfoil and then in tandem configurations.

2.2.1 Dynamic Stall

Lift can be augmented well beyond the maximum static lift coefficient by rapidly changing the incidence of an airfoil, as first noted by Kramer (1932). This process is known as dynamic stall and is best understood for purely-pitching airfoil kinematics, for example as a cause of stall flutter on helicopter rotors, see Leishman (2006). During the dynamic-stall process the viscous effects lag behind the instantaneous angle of attack and the inviscid pressure field. During the rise in lift, the pressure field about the airfoil adjusts to the instantaneous angle of attack at the speed of sound, whereas the viscous effects act at a much slower timescale, as described by Cebeci et al (2005). This delay allows for a huge overshoot in the maximum static lift coefficient, often followed by lift hysteresis with respect to the instantaneous effective angle of attack, as can be seen in Fig. 2.3.

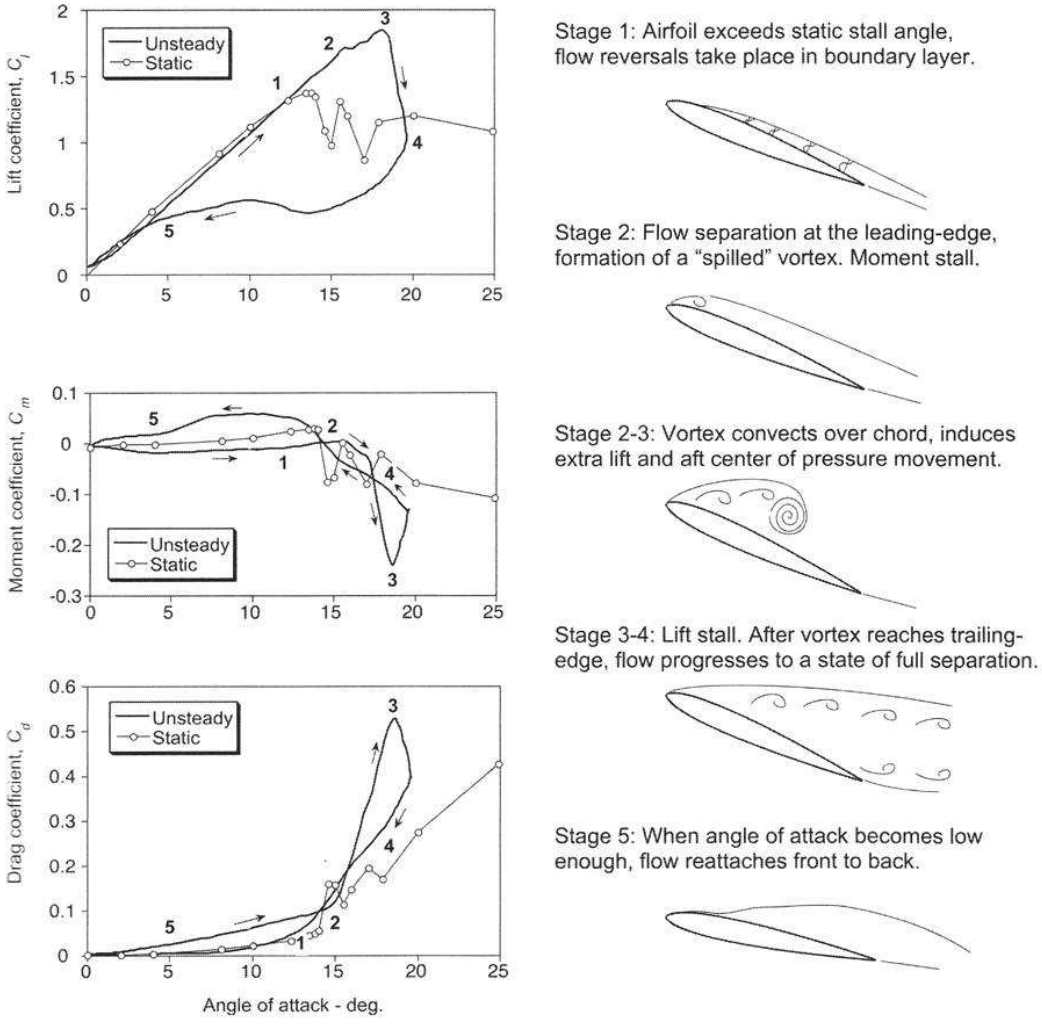

Figure 2.3: Schematic of the dynamic-stall process, from Leishman (2006).

The different stages of the dynamic-stall process for a pitching airfoil are presented in Fig. 2.3. At relatively low mean angles of attack, the first stage is found to be quasi-steady. With increasing angle of attack the lift coefficient rises linearly following an inviscid solution. When approaching the static-stall angle the flow reverses in the boundary layer. However, unlike for the steady case, the flow remains globally attached when crossing the static-stall angle. Stage 2 begins with the formation of a closed separation at the leading edge, in the form of a LEV. At low Mach numbers such as studied here, the LEV can lead to lift values up to 100% higher than the maximum static lift, see Cebeci et al (2005) and Leishman (2006). This is achieved due to low pressure associated with the LEV. The LEV convects over the airfoil surface at approximately

$$0.333 < \frac{u_{conv}}{U_\infty} < 0.5, \tag{2.1}$$

as shown by Beddoes (1976) and Galbraith et al (1986), while growing in strength and increasing lift until it reaches the trailing edge, at which point the separation opens. This marks the beginning of Stage 3 where lift peaks and then drops sharply. Here drag increases due to the fully-separated nature of the flow. After the effective angle of attack drops below the static-stall angle the flow begins to reattach. Once again, the viscous flow lags behind the instantaneous effective angle of attack and reattachment may be delayed substantially. Here the flow typically reattaches from front to back and finally returns to an attached state in Stage 5.

McCroskey (1982) found the key parameters for dynamic stall to be the mean effective angle of attack (α_0) and the reduced frequency (k). The mean angle of attack is the effective incidence about which the motion oscillates. The reduced frequency is a measure of the level of unsteadiness of the flow, as discussed by Cebeci et al (2005). The reduced frequency relates the forcing frequency of the oscillating airfoil to the convective scale of the flow. In this study the reduced frequency is defined in the following manner:

$$k = \frac{\pi f c}{U_\infty}, \tag{2.2}$$

where f is the pitching/plunging frequency, c the airfoil chord and U_∞ the freestream velocity. Mean angle of attack and reduced frequency are indisputably the dominant parameters of the dynamic-stall process. However, to what extent the specific airfoil kinematics impact the vortex formation and pinch-off processes remains virtually unknown and is the subject of chapters 6 and 7.

2.2.2 Stall Regimes

For a given reduced frequency, dynamic stall can be characterized by the maximum effective angle of attack of the motion, see McCroskey (1982). The first category of dynamic stall is referred to as stall onset, for which there is only limited separation. Stall onset represents the maximum unsteady lift that can be achieved, without incurring significant drag and pitching moment penalties. By increasing the maximum effective angle of attack one moves into the light-stall regime. For light stall, separation is on the order of the airfoil thickness and no distinct vortices are formed. Also noteworthy is that for this regime hysteresis is first encountered. Going beyond the maximum effective angle of attack of light-stall results in the vortex-dominated, deep-stall regime. As can be seen in Fig. 2.3, deep stall incurs significant pitch-down moments and drag penalties, particularly as the LEV pinches off at Stage 3 and the flow becomes fully-separated. Deep stall with the conventional sinusoidal airfoil kinematics generally results in significant

hysteresis loops for the lift coefficient. A schematic from McCroskey (1982) with the classification of light and deep stall is presented in Fig. 2.3.

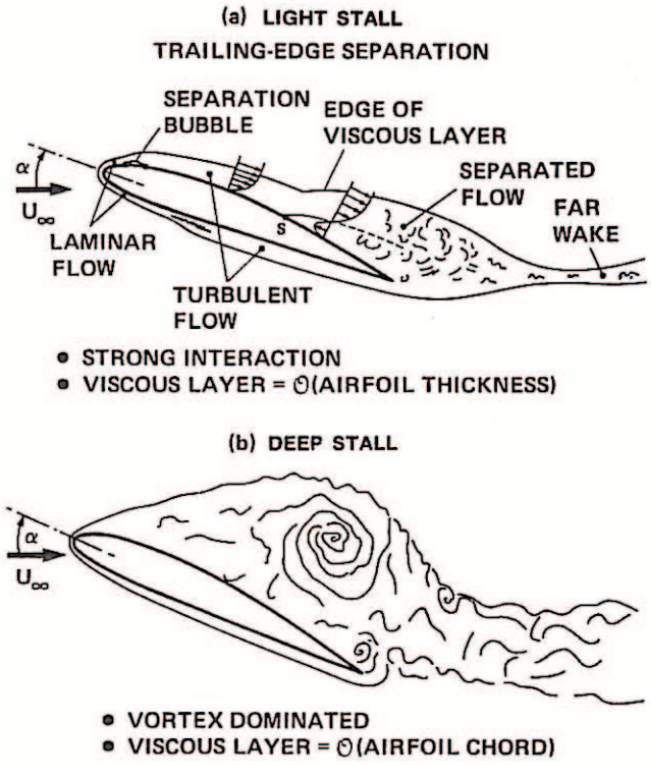

Figure 2.4: Schematic characterizing light and deep stall, from McCroskey (1982).

To-date most studies on dynamic stall have been restricted to sinusoidal kinematics. In chapters 6 and 7, airfoil kinematics have been chosen to minimize the time spent in the fully-separated state. Ideally the fully-separated flow of Stage 4 would be completely bypassed. Whether specific airfoil kinematics can provide relief from the large hysteresis loops by allowing reattachment to occur earlier and more quickly, has been systematically investigated in this thesis.

2.2.3 Leading-Edge Vortex

Thomas et al (2004) visualized the flow around free-flying dragonflies demonstrating the existence of large, quasi two-dimensional leading-edge vortices (LEVs) over their high aspect ratio forewings. Such LEVs can be characterized by a region of strong rotation with a maximum size on the order of the airfoil chord, in turn fed by a shear layer emanating from the leading edge. The production of LEVs is a common mechanism used to augment lift in biological flight and has been studied in detail for pitching airfoils in the context of rotorcraft. Numerous experimental studies exist, particularly related to helicopter aerodynamics, and have been reviewed in detail by Leishman (2006). Carr et al (1977) measured the lift, drag and moment coefficients for a pitching airfoil undergoing dynamic stall and found large hysteresis loops that characterize the lift coefficient curve. Lift augmentation was present, as were peaks in drag and negative aerodynamic moment. For a harmonically plunging and pitching foil Read et al (2003) found instantaneous lift coefficients with values up to 15 and mean lift values over the cycle as high as 5.5. More abstract investigations into LEV formation have been performed by Panda and Zaman (1994) and Ohmi et al (1990) for pitching and pitching/plunging airfoils, respectively.

2.2.4 Trailing-Edge Vortex

In classical inviscid aerodynamics (potential theory), lift L is related to the bound circulation Γ_B through the Kutta-Joukowski theorem

$$L = \rho U_\infty \Gamma_B. \tag{2.3}$$

An increase of circulation around the airfoil results in an augmentation of lift. In order to fulfill Kelvin's law

$$\frac{D\Gamma}{Dt} = 0, \tag{2.4}$$

circulation equal and opposite to the clockwise lift-augmenting circulation must also be produced. For gradual changes in lift, this counter-clockwise circulation is continually shed from the trailing edge in the form of a vortex sheet. For rapid changes in lift, however, the vortex sheet may roll-up into a distinct starting vortex or trailing-edge vortex (TEV), should the pressure difference across the trailing-edge be large enough.

The lift on an impulsively started airfoil in an incompressible inviscid flow was first modeled by Wagner (1925). As the airfoil moves away from the starting vortex, the lift coefficient asymptotes toward the quasi-steady lift coefficient. However, lift remains below 80% of the steady-lift value until the airfoil has traveled approximately three chord lengths, which at $k = 0.25$ (as used in the wind-tunnel measurements) represents a quarter of a cycle. Therefore the TEV has significant lift-diminishing effects for the reduced frequencies studied here. Similarly Kuessner (1936) modeled the airfoil gust response for sharp-edged gusts. In a similar manner to the Wagner function, lift was also found to asymptote to the steady-lift value, but at an even slower rate than that of the Wagner function.

For the strongly separated flows studied here, however, flow visualization by Panda and Zaman (1994) have shown that not only a starting vortex at the trailing edge but also a leading-edge separation in the form of a LEV are produced for harmonic oscillating airfoils with large amplitudes. For this case the TEV is generated through the rolling-up of the trailing-edge shear layer as the LEV convects by. Subsequently the vortex pair has been shown to convect downstream to form the so-called *mushroom-wake* structure. Similar to a starting vortex described above, a TEV is unfavorable to the overall lift production as it counteracts the airfoil circulation (bound vortex). TEV formation is especially detrimental for cyclic motions that produce a TEV on every downstroke, since the relative spacing of the shed vortices to this bound vortex is small. Contrary to the fast convection of a starting vortex, Panda and Zaman (1994) have shown that the mushroom-wake structure asymptotically approaches the free-stream velocity, thus countering the bound vortex for a relatively long period of time during the cycle. As previously mentioned, dragonflies periodically produce a LEV on their forewings. However, Thomas et al (2004) found that no distinct TEV was formed, but rather a shear layer consisting of many smaller TEVs was produced instead. Replacing a large TEV with a shear layer consisting of smaller vortices is beneficial for lift as described by Katz and Plotkin (2001).

In order to satisfy Kelvin's law for the case of full separation, the production of both the positive and negative circulation in the flow must be equal to the net lift. Sources of circulation include the bound vortex as well as vortical structures emanating from both leading and trailing edges. During the growth phase of the LEV, counter-rotating vorticity is continually shed from the trailing edge and Kelvin's law is fulfilled. As the LEV passes over the trailing edge the shear layer rolls up into a distinct vortex. At the same time vorticity is still produced at the leading edge and the flow around the airfoil

develops into a fully-separated state. The lingering flow separation after LEV pinch-off does not increase lift but rather the drag, as discussed in Carr et al (1977), McCroskey (1982) and Leishman (2006).

2.2.5 Reattachment

As described in section 2.2.1, a strong hysteresis in the forces is caused by the delay in reattachment due to the slow viscous time scales. In section 7.2.4 this reattachment process is accelerated through manipulation of the TEV and proves vital to efficient propulsion for flapping flight. Ahmed and Chandrasekhara (1994) studied the reattachment process of an oscillating airfoil typical for helicopter applications with a reduced frequency of $k = 0.05$. They found a slow reattachment process with the flow reattaching from front to rear. Separation was maintained until the effective angle of attack fell well below the static-stall angle. Fast flow reattachment not only reduces the size of the force and moment hysteresis, but more specifically the time spent in the disadvantageous low-lift/high-drag regions of the cycle. Green and Galbraith (1995) found that flow reattachment is comprised of two overlapping mechanisms. The first is a pitch-rate independent convection wave, which is followed by the pitch-rate dependent re-establishment of a boundary layer and fully-attached flow. A more detailed description of the reattachment mechanisms can be found in Sheng et al (2007). For the measurements performed in this thesis, the temporal and spacial resolution does not allow the two mechanisms to be distinguished from each other.

2.3 Vortex Dynamics

2.3.1 Optimal Vortex Formation

The dimensionless vortex formation time $\hat{T}$, often referred to as simply the formation time, is a measure of the state of development of a vortex. In a review paper on this topic, Dabiri (2009) suggests the existence of a level of universality among all unsteady vortical flows through the concept of an optimal vortex formation number, where the vortex stops entraining fluid from the shear layer and pinches off at a value of $\hat{T} \approx 4$. The formation time is defined in its general form in the following manner:

$$\hat{T} = \frac{C\Gamma}{D\Delta U}, \tag{2.5}$$

where C is a constant factor depending on the physical configuration of the vortex generator, Γ is the instantaneous vortex strength, D the characteristic length scale and ΔU the shear-layer feeding velocity. For the specific case of a two-dimensional plunging airfoil with only one LEV shed per cycle, the vortex generator constant has been set to $C = 1$ and the limiting length scale of the forming vortex set as $D = 2c$. The shear-layer feeding velocity was approximated by $\Delta U = 2\pi f h_o$, being the maximum plunge velocity of the airfoil leading edge over the downstroke. Milano and Gharib (2005) showed that maximum lift on a pitching and plunging plate was generated when $\hat{T} \approx 4$, such that the LEV would pinch off just at the end of the half stroke. A follow-up study using a translating low-aspect-ratio plate with a start-up motion was performed by Ringuette et al (2007) to better understand the impact of the tip vortex in the start-up process. Again the LEV was found to pinch off at around $\hat{T} \approx 4$. This universal behavior in the formation of the LEV is a focus throughout this thesis, with close attention being given

to the influence of the airfoil kinematics and the presence of the hindfoil on this pinch-off process.

Further to this, it has been shown that vorticity can be entrained beyond the formation number $\hat{T} = 4$ by varying piston kinematics and nozzle diameter in vortex generators, as shown by Dabiri (2005) and Shusser et al (2006). Although vortex generation on a dynamic airfoil is somewhat more complex than that of a vortex ring generator, it is expected that similar results can be achieved for the dynamic-stall process on an airfoil. Both single and tandem airfoil kinematics may possibly be used to increase the formation number and therefore the maximum circulation of the LEV. These results are presented in sections 6.3.4, 9.2.3 and 9.3.3.

2.3.2 Vortex Convection

Based on the reduced frequency of $k = 0.25$ used for most of the wind-tunnel tests in this thesis, a particle of fluid moving at U_∞ would convect $x/c \approx 12.5$ over one full period of the plunging motion. Panda and Zaman (1994) have shown that the actual convection speed (u_{conv}) of shed vortices varies between

$$0.6 < \frac{u_{conv}}{U_\infty} < 0.8 \tag{2.6}$$

in the vicinity of the airfoil, largely dependent on the position, size and strength of the vortex. These vortices then rapidly accelerate to the free-stream velocity in the immediate wake. Therefore one can infer that a LEV shed at the bottom of the plunge stroke would travel $x/c \approx 6$ in the time that the airfoil would require to return back to the top of the stroke. This relatively large spacing between the LEVs suggests that the history effects in the dynamic-stall process are not strongly influenced by the previous cycle's shed vortices in the wake. Rather the history effects are expected to be more strongly influenced by the slow time scales associated with boundary-layer separation and reattachment present in the dynamic-stall process itself. In other words the state of the boundary-layer at the top of the stroke, just before the LEV formation process begins, should play a much larger role than the LEV shed from the previous cycle. A further discussion on these history effects is treated in Section 6.2. Measurement and comparison of these history effects are then presented in Section 6.3.2.

When considering the influence of vortex convection for the tandem hover configuration in chapter 10, the vortex induction in contrast plays a dominant role on the vortex trajectories. Here the shed vortices linger in the general vicinity for as long as a full period and therefore influence further vortex development and therefore the instantaneous forces substantially. An overview of such wake-capture effects in hover is given in Birch and Dickinson (2003).

2.3.3 Blade-Vortex Interaction

The interaction between a vortex and an arbitrary body can be characterized by the orientation of the vortex (parallel, streamwise or normal) as well as the proximity at which the vortex passes, i.e. inviscid versus viscous interaction. A large body of analytical, numerical and experimental studies exists in the literature and has been reviewed in great detail by Rockwell (1998). Parallel blade-vortex interaction, a subset of vortex-body interactions examined extensively by Wilder and Telionis (1998), occurs in a wide spectrum of applications and Reynolds numbers. For high Reynolds-number applications ranging from rotorcraft and wind turbines, it is often adequate to use an inviscid

treatment as in Yao and Liu (1998). However, at the other end of the spectrum, when examining the flow of miniaturized flapping drones referred to as Micro Air Vehicles (MAVs), large separations are inevitable, as described in Mueller (2001). For such cases the dynamic pressures are extremely low, i.e. $\Delta p = \mathcal{O}(10\text{Pa})$, such that the integration of fast-response miniaturized pressure sensors in small wind-tunnel models becomes impractical. Therefore a shift to velocity-field measurements such as PIV is necessary to quantitatively examine such interactions at these low Reynolds numbers. In fact, in stark contrast to pressure measurements, the accuracy of pressure extraction using PIV remains insensitive to flow velocity magnitude, as discussed by van Oudheusden et al (2007). This methodology is treated in section 3.11.

2.4 Energy Recovery

When evaluating the performance of a propulsive system, one usually considers the overall propulsive efficiency defined as:

$$\eta_P = \frac{tU_\infty}{P}, \tag{2.7}$$

where t is the thrust, U_∞ the velocity of the system and P the power exerted on the surrounding fluid. It therefore becomes clear that to maximize the propulsive efficiency, one needs to simultaneously address the two independent quantities of thrust and power. These two factors in the context of unsteady tandem configurations will now be discussed, first examining thrust production through *leading-edge suction* and then power reduction through *normal suction*.

2.4.1 Thrust Production

Knoller (1909) and Betz (1912) were the first to postulate that a plunging symmetric airfoil can create not only lift but also thrust, generalizing this effect as a consequence of the horizontal component of the lift force when the airfoil is plunged up or down, as shown in Fig 2.5. Katzmayr (1922) subsequently verified the so-called *Knoller-Betz* effect in his wind-tunnel experiments, where he measured the thrust force exerted on an airfoil in a wavy wake.

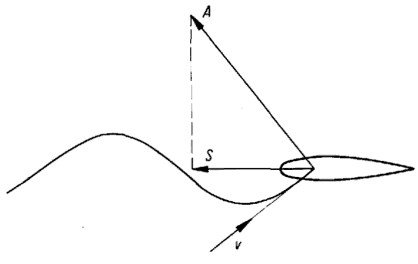

Figure 2.5: Creation of thrust on a plunging airfoil, where A is the lift force and S is the resulting horizontal component; taken from Schmidt (1965).

Schmidt (1965) tested a tandem-airfoil configuration in which the wake of the rotating forefoil was used to produce thrust on the static hindfoil. This propulsion system was referred to as a *Wellpropeller*, translated as wave propeller. Using a hindfoil profile geometry with a maximum thickness-to-chord ratio of $t/c = 0.25$, the best results were achieved. Compared to conventional airfoils the relatively thick profile was beneficial in creating high thrust forces through the so-called leading-edge suction effect. This

suction bubble, which is developed through a strong flow acceleration at the leading edge, is described in detail for static airfoils by Katz and Plotkin (2001). Although Schmidt's experiments were performed at reduced frequencies of $1 \leq k \leq 4$, i.e. at one order of magnitude higher than the experiments in this study, similar trends can be expected. Furthermore, any details regarding this thrust-producing mechanism were not measured for this configuration and are therefore uncovered in chapters 8 and 9.

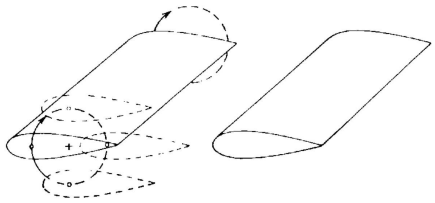

Figure 2.6: Arrangement and kinematics of airfoils used for the wave-propeller experiments; taken from Schmidt (1965).

Warkentin and DeLaurier (2007) tested a tandem-wing ornithopter configuration with reduced frequencies in the range of $0.4 \leq k \leq 1$. They found that a close spacing of approximately one chord length between the wings and phase angles between $\psi = 0\,^\circ$ and $\psi = 50\,^\circ$ were most beneficial for thrust efficiency. A synergy due to the tandem-wing interactions was obtained such that the propulsive efficiency was at times double that of the single-airfoil reference case, even when taking the larger reference area of the tandem arrangement into consideration. Furthermore it was hoped that asymmetric flapping at phase angles of $\psi = 180\,^\circ$ would produce high thrust efficiencies and simultaneously minimize vertical accelerations for a given MAV design. Unfortunately this phasing presented a substantial drop in performance. Significant leading-edge suction for a static hindwing, based on Schmidt's wave-propeller configuration, could not be achieved in this experiment. A possible explanation for this is the geometry of the thin membrane wings used in the study with their sharp leading edges, thus not providing the necessary surface area for the suction force. Again no details pertaining to the flow field at the hindwing leading edge were measured.

2.4.2 Power Reduction

The aerodynamic power consumption (P) for a pitching and plunging airfoil over a given period (T) is defined as:

$$P = \frac{1}{T} \int_T (L\dot{h} + M\dot{\alpha}) dt, \tag{2.8}$$

where the moment (M) term can be neglected due to the relatively low pitch velocities ($\dot{\alpha}$). Subsequently the nondimensional power coefficient can be defined as follows:

$$C_P = \frac{2P}{\rho {U_\infty}^3 c}. \tag{2.9}$$

In the case of hover, the maximum plunge velocity ($\dot{h}_{max}$) is used to nondimensionalize en-lieu of the free-stream velocity (U_∞).

Akhtar et al (2007) showed that bluegill sunfish could modify their thrust production but also their side forces through the interaction of the dorsal-fin wake on the tail fin. During a distinct phasing between the two fins, the effective angle of attack could be increased at the tail fin such that a much stronger LEV was established. The stronger

LEV was found to increase the suction on the side of the fin. Similarly the studies of Gopalkrishnan et al (1994) revealed vortex energy capture by a foil in the wake of a D-shaped cylinder, mimicking the behavior of trout in fast-moving water. Here particular modes of vortical interaction were observed such that the vortices from the cylinder interacted with the vortices shed by the foil. For the case of *destructive interaction*, cylinder vortices were repositioned and weakened by vorticity produced by the foil, thus maximizing propulsive efficiency. As a follow-up to this work, Beal et al (2006) showed that euthanized trout (or an analogous passively-mounted foil) could travel upstream (produce thrust) without any power input. This passive propulsion was possible through simple reorientation of the oncoming vortical energy shed from the upstream cylinder. This latter study is an excellent example of how both thrust production through leading-edge suction and vortical-energy extraction through normal suction are coupled and strongly dependent on vortex-airfoil phasing.

As an extension to this concept of energy harvesting through normal suction, studies by McKinney and DeLaurier (1981), Kinsey and Dumas (2006) and Platzer et al (2009) all have investigated the capacity of a pitching/plunging foil to extract energy from a stream through aerodynamic flutter. The latter study has shown substantial improvements when positioning a second moving foil in the wake. Further to this, Zhu and Peng (2009) recently showed that the development of the LEV and its subsequent convection over the foil surface can be used to develop a strong pitch-down moment, which in turn can be used for power extraction. Finally, Dabiri (2007) developed a model based on vortex dynamics showing that the energy extraction mechanism is a function of the oncoming vortex positioning and strength relative to the body. Unfortunately, such a treatise is often too simple for use in the highly-separated flow field associated with dragonfly flight.